

Impacts of Convectively Coupled Kelvin Waves on Environmental Conditions for Atlantic Tropical Cyclogenesis

MICHAEL J. VENTRICE AND CHRISTOPHER D. THORNCROFT

Department of Atmospheric and Environmental Science, University at Albany, State University of New York, Albany, New York

CARL J. SCHRECK III

Cooperative Institute for Climate and Satellites, North Carolina State University, Asheville, North Carolina

(Manuscript received 31 October 2011, in final form 2 February 2012)

ABSTRACT

High-amplitude convectively coupled equatorial atmospheric Kelvin waves (CCKWs) are explored over the tropical Atlantic during the boreal summer (1989–2009). Focus is given to the atmospheric environmental conditions that are important for tropical cyclogenesis.

CCKWs are characterized by deep westerly vertical wind shear to the east of its convectively active phase and easterly vertical wind shear to the west of it. This dynamical signature increases vertical wind shear over the western tropical Atlantic ahead of the convectively active phase, and reduces vertical wind shear after its passage. The opposite is true over the eastern tropical Atlantic where the climatological vertical wind shear is easterly.

Positive total column water vapor (TCWV) anomalies progress eastward with the convectively active phase of the CCKW, whereas negative TCWV anomalies progress eastward with the convectively suppressed phase. During the passage of the convectively active phase of the CCKW, a zonally oriented strip of low-level cyclonic relative vorticity is generated over the tropical Atlantic. Two days later, this strip becomes more wavelike and moves back toward the west. This signature resembles a train of westward-moving easterly waves and suggests CCKWs may influence such events.

Strong CCKWs over the tropical Atlantic tend to occur during the decay of the active convection associated with the Madden–Julian oscillation over the Pacific. This relationship could be used to provide better long-range forecasts of tropical convective patterns and Atlantic tropical cyclogenesis.

1. Introduction

Tropical cyclones commonly form when sea surface temperatures are warm and when large-scale environmental conditions (e.g., low-moderate vertical wind shear, increased low-to-midlevel moisture, and sufficient low-level cyclonic relative vorticity) are favorable for tropical cyclogenesis (Gray 1968, 1988, 1998). Such conditions are known to vary on different time scales. At multidecadal time scales, the environment over the Atlantic has been shown to vary with the Atlantic multidecadal oscillation (AMO; e.g., Klotzbach and Gray 2008; Aiyyer and Thorncroft 2011). At interannual time

scales, the environment is modulated according to the particular phase of the El Niño–Southern Oscillation (ENSO; e.g., Gray 1984; Goldenberg and Shapiro 1996). At intraseasonal time scales, the Madden–Julian oscillation (MJO) provides periods of favorable or unfavorable conditions over the Atlantic (e.g., Maloney and Shaman 2008; Klotzbach 2010; Ventrice et al. 2011). Additionally, a period of favorable environmental conditions might only last for a few days and still yield a tropical cyclone. These subseasonal periods of favorable conditions might be provided by convectively coupled equatorial atmospheric Kelvin waves (CCKWs).

CCKWs are eastward-propagating atmospheric waves that are found to substantially modulate tropical rainfall on synoptic spatial and temporal scales (Gruber 1974; Zangvil 1975; Takayabu 1994; Wheeler and Kiladis 1999; Wheeler et al. 2000; Mekonnen et al. 2008). This modulation of rainfall is found to occur primarily along

Corresponding author address: Michael Ventrice, University at Albany, State University of New York, 1400 Washington Ave., Albany, NY 12222.
E-mail: mventrice@albany.edu

the latitude of the climatological intertropical convergence zone (ITCZ), which exists between the equator and 15°N over the central-eastern Pacific and Atlantic basins (Kiladis et al. 2009). Over Africa and South America, the ITCZ varies more substantially with season (Roundy and Frank 2004). CCKWs significantly modulate the diurnal cycle of convection and mesoscale convective systems (MCSs), which is most evident over the Atlantic and African regions (e.g., Mounier et al. 2007; Nguyen and Duvel 2008; Kiladis et al. 2009; Laing et al. 2011). Most of the organized rainfall within the eastward-moving envelope of a CCKW appears to be associated with smaller-scale cloud clusters that move westward (e.g., Straub and Kiladis 2002; Mekonnen et al. 2008; Kiladis et al. 2009; Kikuchi and Wang 2010; Laing et al. 2011). Kiladis et al. (2009) found that some of the westward propagation can be accounted for by an easterly basic state. In many cases, however, the westward phase speeds are too fast to be explained by advection alone. These fast westward-moving disturbances are likely associated with westward inertio-gravity waves (Tulich and Kiladis 2012).

Over the tropical Atlantic and African regions, CCKWs propagate eastward with an average phase speed of about 15 m s^{-1} and an associated average wavelength of about 8000 km (Mounier et al. 2007). The passage of the convectively active phase of the wave is preceded by low-level easterly wind anomalies and is followed by low-level westerly wind anomalies. Maximum low-level zonal convergence is located about 15° of longitude to the east of the OLR minima (Takayabu and Murakami 1991; Straub and Kiladis 2002). The upper-level flow associated with CCKWs over Africa is generally zonal as predicted by linear shallow-water theory (Matsuno 1966), but substantial meridional flow associated with the passage of a CCKW exists over the tropical Atlantic (Ventrice et al. 2012). This upper-level meridional flow is associated with an off-equatorial convective signal over the northern equatorial Atlantic. Dias and Pauluis (2009) performed an idealized modeling study that demonstrated CCKWs propagating along a narrow precipitation region can produce a meridional circulation. This meridional circulation modulates both the amount of precipitation and the horizontal extent of the ITCZ, which can affect the phase speed of the CCKW. Further observational evidence of meridional flow composing the dynamical structure of a CCKW is provided over Africa (Mounier et al. 2007), over the Indian Ocean (Roundy 2008), and over the east Pacific (Straub and Kiladis 2003c).

The geographical distribution of Kelvin-filtered OLR variance [averaged over 1979–2009 for June–September (JJAS)] is shown in Fig. 1. The overall activity is similar

to previous studies using Kelvin-filtered OLR variance (e.g., Wheeler and Kiladis 1999; Wheeler et al. 2000; Roundy and Frank 2004; Mekonnen et al. 2008; Kiladis et al. 2009). Peak activity occurs over the equatorial Indian Ocean and northern equatorial west-central Pacific. Kelvin wave activity is also observed generally between 5°–10°N over the entire tropical central-to-eastern Pacific and Atlantic Oceans and along 10°N over West Africa. The Kelvin-filtered OLR variance is not symmetric about the equator except for over the Indian Ocean, consistent with the previous analyses of Kelvin wave variance (e.g., Straub and Kiladis 2002; Roundy and Frank 2004; Mekonnen et al. 2008). Over the Atlantic, Kelvin wave OLR variance is observed north of the equator and is characterized by slightly weaker magnitudes compared to the rest of the tropical band.

Ventrice et al. (2012) discussed the genesis of Tropical Storm Debby (2006). A weak African easterly wave (AEW) initially strengthened in association with the coherent diurnal cycle of convection found downstream of the Guinea Highlands region. It later formed into a tropical cyclone during the superposition with an eastward-propagating CCKW. They also investigated the climatological modulation of Atlantic tropical cyclogenesis by CCKWs. Tropical cyclogenesis was less frequent 1–2 days prior to the passage of the convectively active phase of the CCKW. Tropical cyclogenesis became more frequent during this passage and peaked just after. The relationship between CCKWs and tropical cyclogenesis frequency found by Ventrice et al. (2012, see their Figs. 8 and 9) provides motivation to investigate the influences of the CCKW on the large-scale environment for tropical cyclogenesis over the tropical Atlantic.

In addition to the direct enhancement of convection by the CCKW, this lead–lag relationship suggests that CCKWs may also change the large-scale environment over the main development region (MDR; 5°–25°N, 15°–65°W). The purpose of this paper is to explore the extent to which CCKWs alter this environment. This study will focus on the influence of CCKWs on the large-scale environmental conditions over the tropical Atlantic that are known to impact tropical cyclogenesis (vertical wind shear, moisture, and low-level relative vorticity). This aspect differs from previous studies that investigate CCKWs over the tropical Atlantic and West Africa (e.g., Mounier et al. 2007; Wang and Fu 2007; Mekonnen et al. 2008), who investigate the convective influence of CCKWs.

The article is structured as follows. Section 2 provides datasets and methodologies. Section 3 discusses a composite analysis highlighting the role of CCKWs on large-scale environment over the tropical Atlantic and West Africa. A discussion relating the large-scale

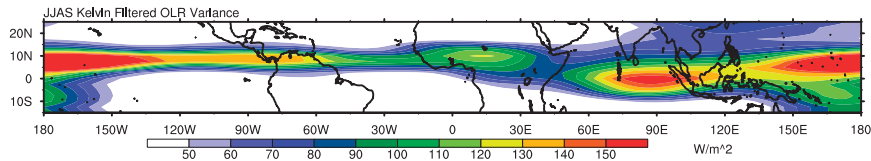


FIG. 1. Distribution of JJAS mean variance of NOAA-interpolated OLR filtered for the Kelvin band. Kelvin wave activity is determined by filtering OLR in the period of 2.5–20 days with eastward wavenumbers 1–14. The filter is constrained by the Kelvin wave dispersion curves for equivalent depths of 8–90 m.

environment modulation associated with CCKWs and tropical cyclogenesis is provided in section 4. Concluding remarks are given in section 5.

2. Data and methodology

The European Centre for Medium-Range Weather Forecasts (ECMWF) Re-Analysis (ERA-Interim) dataset (Simmons et al. 2007) was used to investigate the synoptic evolution of the composited CCKW. This dataset covers the period 1989 to the present and has a horizontal resolution of 1.5° . Previous studies (e.g., Kiladis et al. 2009 and references therein) have shown the utility of similar reanalyses for studying the structures of equatorial waves.

Convection associated with CCKWs is explored using the National Oceanic and Atmospheric Administration (NOAA) daily averaged interpolated OLR dataset, with a horizontal gridded resolution of 2.5° (Liebmann and Smith 1996). To support the analysis of CCKWs, wavenumber-frequency filtering was applied on the daily averaged NOAA-interpolated OLR dataset following the methodology of Wheeler and Kiladis (1999). Filtering for the Kelvin wave was performed with a period range of 2.5–20 days, with eastward wavenumbers 1–14. The filter is constrained by the Kelvin wave dispersion curves for equivalent depths of 8–90 m. This methodology has been demonstrated similarly in Straub and Kiladis (2002) and Mekonnen et al. (2008). In short, this methodology decomposes a field of data into wavenumber-frequency components for eastward-moving wave disturbances. Before the decomposition, the data are detrended and the ends of the time series were tapered to zero to control spectral leakage [see Wheeler and Kiladis (1999) for additional details].

Following the methodology of Ventrice et al. (2012), a time series was developed based on a selected grid point over the tropical Atlantic (10°N , 15°W) selecting all days where the minimum Kelvin-filtered negative OLR anomalies were less than -1.5 standard deviations in magnitude during the 1989–2009 JJAS seasons. The latitude of the base point was selected north of the equator where the highest JJAS Kelvin-filtered OLR

variance is found over the coast of West Africa (Fig. 1). The longitude of the base point is selected because of our interest in the relationship with tropical cyclones. This base point is different to the location chosen by Mekonnen et al. (2008), who chose their point in association to where the greatest variance is found over Africa. A total of 142 CCKWs were objectively identified using this methodology. Lags were then used on this time series in order to examine propagating characteristics. For clarification, “day 0” is when the minimum composited Kelvin-filtered OLR anomaly moves over the selected base point.

Anomalies for all composited fields were constructed by subtracting the long-term mean and the first four harmonics of the seasonal cycle. Bootstrap random resampling tests with 1000 iterations were used for statistical significance testing on all anomalies similar to Roundy and Frank (2004). In each of these tests, a new sample equal in size to the original was randomly drawn for the original set of composite dates with replacement. The composite anomalies were considered 90% significant if 900 out of the 1000 random composites had the same sign.

3. Composite analysis of convectively coupled Kelvin waves over the Atlantic

a. The vertical structure

The distinctive vertical structure of the CCKW is highlighted in Fig. 2 using the ERA-Interim reanalysis data. This figure is sampled when the composite minimum negative Kelvin-filtered OLR anomaly is located over 15°W . The cross section is averaged over the latitudinal band 5°S – 10°N to maximize the signature of the CCKW within the selected fields. The resulting vertical structure compares remarkably well with the time–height composites of Straub and Kiladis (2003c) and Kiladis et al. (2009), who used 12-hourly radiosonde data over the Pacific island of Majuro (7.1°N , 171.4°E).

The zonal wind–height cross-section composite illustrates a strong westward tilt with height of weak zonal wind anomalies through the lower troposphere and an eastward tilt with height of higher-amplitude zonal wind

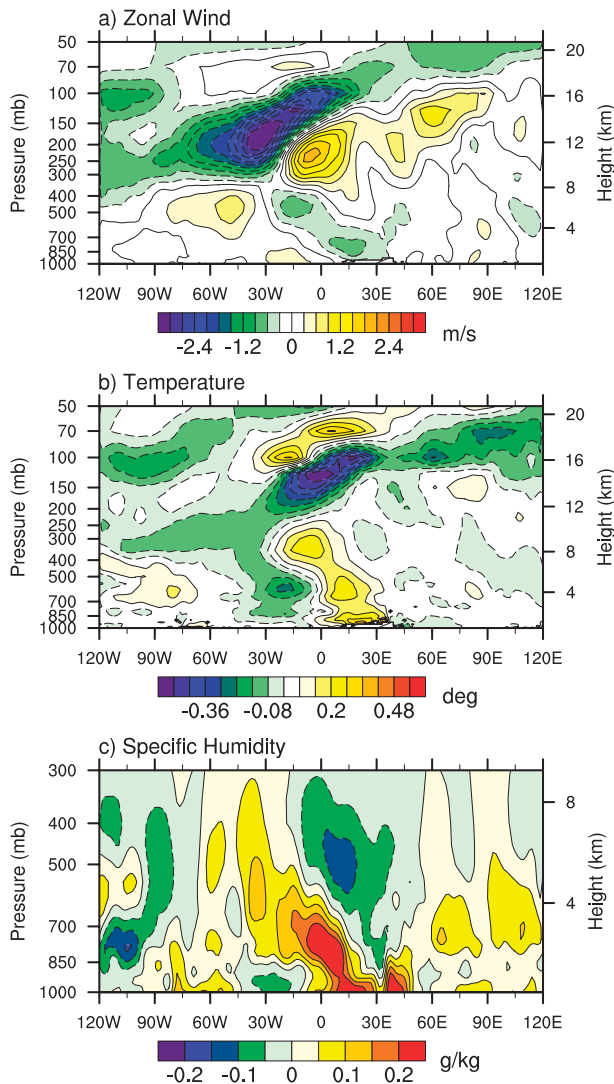


FIG. 2. Height-longitude cross-sectional composite averaged over the 5°S – 10°N latitude band for anomalies of (a) zonal wind, (b) temperature, and (c) specific humidity. The minimum Kelvin-filtered OLR anomaly is located at the longitude of 15°W .

anomalies in the upper troposphere and lower stratosphere (Fig. 2a). In agreement with Straub and Kiladis (2003a,c), low-level (850 hPa) zonal wind convergence is observed to precede upper-level (250 hPa) divergence by roughly 15° of longitude. The most dominant wind signature is located in the upper troposphere, highlighted by strong westerly anomalies between 15°W and 15°E and strong easterly wind anomalies between 30° and 60°W . These easterly wind anomalies over 30° – 60°W are observed throughout the 100–300-hPa layer and extend westward through 120°W . Therefore, a deep layer of anomalous upper-level easterly flow exists over the tropical Atlantic after the passage of the CCKW. This anomalous upper-level easterly flow extends well

over 90° of longitude (15° – 120°W) and exists over a deep layer (700–400 hPa) of anomalous westerly flow.

The temperature (Fig. 2b) and specific humidity (Fig. 2c) cross sections display vertical structures similar to the observations of Kiladis et al. (2009). Lower-tropospheric moistening begins over 30°E and extends back westward with height, becoming vertical in nature over 15°W . Simultaneously, a warming of the lower troposphere occurs represented by the positive temperature anomaly beginning in the lower troposphere over Africa, extending back westward with height to 300 hPa over 10°W . Over the longitudes of 15°W – 0° , the lower troposphere begins to dry and cool, while the mid- to upper troposphere remains moist and warm in association with deeper convection. The broad cold anomaly extending from 850–500 hPa at 15°W is associated with adiabatic cooling due to vertical ascent. In contrast to observations of Straub and Kiladis (2003c) and Kiladis et al. (2009), no cold pool exists near the surface over 15°W , which is attributed to a lack of convective cold downdrafts reaching the surface. This result might arise from the location of the composite, sampling the moist Atlantic ITCZ, or it could represent a shortcoming of the model-derived reanalysis. The vertically stacked oriented lines of negative and positive temperature anomalies that tilt eastward with height between the 200–50-hPa layer over 15°W highlights the upward propagation of wave energy, which is consistent with an eastward-moving upper-tropospheric heat source (Lindzen 1967; Lindzen and Matsuno 1968; Andrews et al. 1987) and with the observations of Straub and Kiladis (2003c) and Kiladis et al. (2009).

The temperature and moisture evolution is also linked to the morphology of cloudiness highlighted in Straub and Kiladis (2002). This morphology begins with shallow convection over 10°E , progressing to deep convection over 15°W , and finally stratiform cloudiness which is associated with a moist upper troposphere and dry lower troposphere over 30°W . The area of cold anomalies below 850 hPa over 15° – 30°W highlights the evaporation of stratiform precipitation in the low-level drier air.

b. The large-scale environmental signature

1) VERTICAL WIND SHEAR

The vertical wind structure of the observed CCKW over the tropical Atlantic is characterized by upper-tropospheric winds opposite to those in the lower troposphere (recall Fig. 2a). Therefore, CCKWs are expected to impact the vertical wind shear patterns over the MDR. The JJAS climatological 925–200-hPa vertical wind shear pattern over the tropical Atlantic, including portions of South America and West Africa is shown in Fig. 3. The direction of shear represents the vector

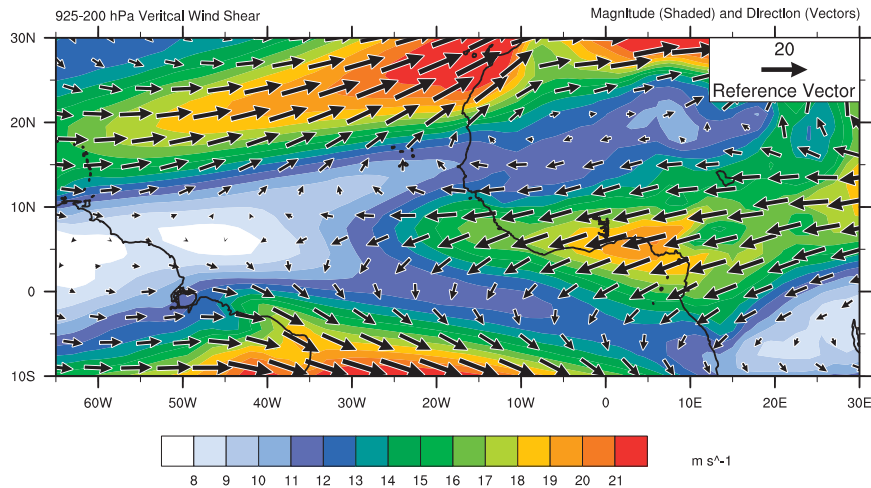


FIG. 3. The JJAS climatological 925–200-hPa vertical wind shear vectors and magnitudes (shaded). The direction of shear represents the vector difference between 925 and 200 hPa.

difference between 925 and 200 hPa. Consistent with results of Aiyyer and Thorncroft (2011), this figure shows that the tropical Atlantic is characterized by two different background vertical wind shear states. The western tropical Atlantic is characterized by westerly vertical wind shear associated with the subtropical westerly jet, whereas a large portion of the eastern tropical Atlantic is characterized by easterly vertical wind shear associated with the tropical easterly jet.

To investigate the influence of CCKWs on synoptic-scale vertical wind shear patterns over the tropical Atlantic, Fig. 4 shows composites of 925–200-hPa vertical wind shear magnitude anomalies (shaded) and vector anomalies (vectors) averaged over each lag of the CCKW index. As in Fig. 3, the direction of shear represents the vector difference between 925 and 200 hPa. At day -6 , westerly shear vector anomalies occur within and to the east of the convectively suppressed phase of the composited CCKW over the western tropical Atlantic (Fig. 4a). These westerly shear vector anomalies shift eastward with time over the tropical Atlantic between the leading convectively suppressed and convectively active phase of the CCKW (Figs. 4a–e). At day -2 , an anomalous anticyclonic shear signature develops within the convectively active phase of the CCKW and highlights the atmospheric response to diabatic heating associated with deep convection (e.g., Ferguson et al. 2009; Dias and Pauluis 2009; Fig. 4e). This anomalous anticyclonic signature is consistent with the composite upper-level wind structure of the CCKW over the Atlantic at this particular time (see Fig. 5 in Ventrice et al. 2012). At day -1 , the anomalous anticyclonic shear signature is now located just west of the minimum Kelvin-filtered OLR anomaly, resembling a Gill–Matsuno-type

response to deep convection (Gill 1980). Furthermore, at this time, northeasterly shear vector anomalies are to the west of the convectively active phase of the CCKW and extend westward over South America (Fig. 4f). Thereafter, easterly shear vector anomalies are observed to progress eastward behind the convectively active phase of the CCKW, consistent with dynamical structure of the CCKW (recall Fig. 2b).

It is important to realize that a particular phase of a CCKW affects the magnitude of vertical wind shear differently depending on the direction of the environmental background wind shear. To illustrate this point, we focus on the westerly vertical wind shear phase of the CCKW over the western tropical Atlantic at day -4 (Fig. 4c). The background westerly shear over South America (Fig. 3) significantly increases within the westerly shear phase ahead of the convectively active phase of the CCKW. Vertical wind shear also significantly increases over the entire tropical North Atlantic poleward of 10°N . Figure 3 shows that these are regions where the climatological vertical wind shear is westerly. Therefore the westerly vertical wind shear phase of the CCKW is acting to increase the background westerly shear over these regions. In contrast to this, over the eastern tropical Atlantic where the climatological shear is easterly (Fig. 3), significantly reduced vertical wind shear is observed equatorward of 10°N within the westerly shear phase of the CCKW (Fig. 4c). The westerly vertical wind shear phase of the CCKW opposes the climatological easterly shear and reduces the background vertical wind shear there. While on day 0, vertical wind shear reduces over South America and over the western tropical Atlantic as the easterly shear phase of the CCKW reduces the climatological westerly shear there

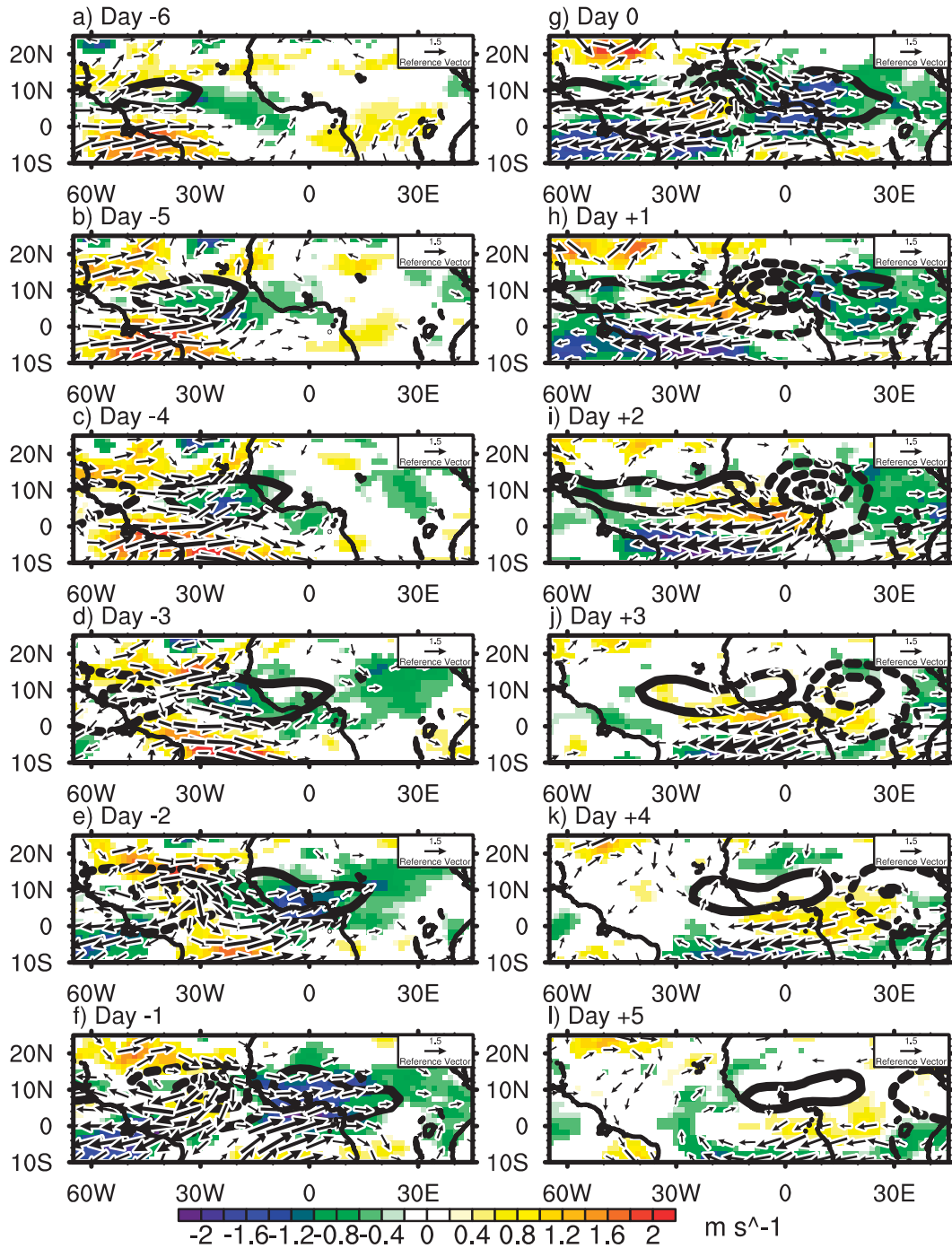


FIG. 4. The 925–200-hPa vertical wind shear vector and magnitude (shaded) anomaly composite averaged over each CCKW lag. Wind shear magnitude anomalies statistically different than zero at the 95% level are shaded. The direction of shear represents the vector difference between 925 and 200 hPa. Vectors are not drawn if less than 0.75 m s^{-1} . Kelvin-filtered OLR anomalies are contoured if statistically different than zero at the 95% level. Negative Kelvin-filtered OLR anomalies are dashed. Shade interval is 0.2 m s^{-1} ; contours begin at $\pm 3 \text{ W m}^{-2}$; contour interval is 6 W m^{-2} ; reference vector is 1.5 m s^{-1} .

(Fig. 4g). Vertical wind shear is also reduced over Africa and poleward of 10°N over the tropical Atlantic for the same reason. Between 0° and 10°N over the eastern tropical Atlantic, vertical wind shear increases as the easterly shear phase of the CCKW increases the climatological easterly shear there. Throughout the subsequent lags (day +1 through day +5), vertical wind shear increases over equatorial Africa as the easterly shear phase of the CCKW increases the climatological easterly there (Figs. 4h–l).

To elaborate on the influence of the CCKW on the vertical wind shear magnitude anomaly over the tropical Atlantic, Fig. 5 shows a time–longitude plot of 925–200-hPa vertical wind shear magnitude anomalies averaged within the 0° – 25°N band over each lag of the CCKW index. Day 0 now represents the time when the minimum composited Kelvin-filtered OLR anomaly passes over a grid point located in the central MDR (10°N , 45°W). A quadrupole signature is apparent within the vertical wind shear magnitude anomaly field. Where the climatological background shear is westerly over the MDR (30° – 65°W), four days prior to the passage of the convectively suppressed phase of the CCKW, vertical wind shear begins to increase. Wind shear magnitude anomalies continue to amplify just before the passage of the minimum Kelvin-filtered OLR anomaly. But directly after the passage of the minimum Kelvin-filtered OLR anomaly, shear is reduced. These negative wind shear magnitude anomalies are smaller in amplitude than the positive wind shear magnitude anomalies observed prior to the passage of the minimum Kelvin-filtered OLR anomaly, but they remain weakly negative up to four days after the passage of minimum Kelvin-filtered OLR anomaly.

Where the climatological background shear is easterly over the MDR, including West Africa (30°W – 0°), the opposite vertical wind shear evolution is observed. Roughly 3–4 days before the passage of the convectively active phase of the composited CCKW, vertical wind shear magnitude anomalies become negative. Wind shear magnitude anomalies over this region remain negative until the passage of the minimum Kelvin-filtered OLR anomaly. Tropical Storm Debby (2006) formed within the convectively active phase of a CCKW over the eastern Atlantic (Ventrice et al. 2012). Vizy and Cook (2009) found that the pre-Debby AEW experienced 40% less vertical wind shear over the coast of West Africa when compared to the preceding AEW (pre Ernesto). This reduction of vertical wind shear over the pre-Debby AEW over the coast of West Africa corresponds well to where the vertical wind shear is expected to be reduced by the CCKW. After the passage of the convectively active phase of the composited CCKW over the eastern

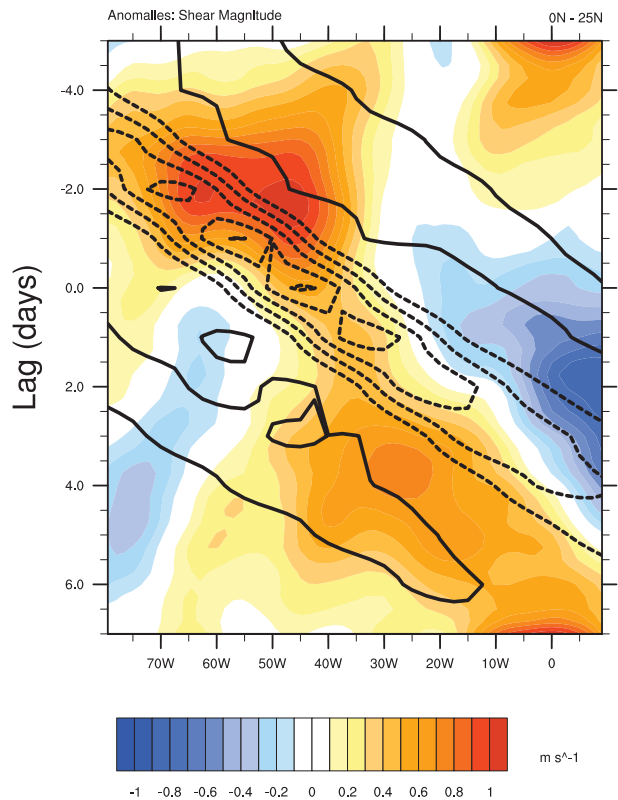


FIG. 5. A time–longitude composite of mean absolute value of anomalous 925–200-hPa vertical wind shear of the total wind averaged over each CCKW lag and the 0° – 25°N latitude band. A 5-day running average was applied to temporally smooth the data. Kelvin-filtered OLR anomalies are contoured if statistically different than zero at the 95% level. Negative Kelvin-filtered OLR anomalies are dashed. Kelvin-filtered OLR anomalies are averaged over the 5° – 10°N latitude band. “Day 0” is when the minimum Kelvin-filtered OLR anomaly moves over 10°N , 45°W . Shade interval is 0.1 m s^{-1} ; contour interval is 3 W m^{-2} .

MDR, vertical wind shear magnitude anomalies become positive and remain anomalously strong up to four days and beyond.

2) ATMOSPHERIC MOISTURE

The relationship between atmospheric moisture and CCKWs is now investigated. Roundy and Frank (2004) found that total column water vapor (TCWV) does not project strongly onto the Kelvin band. However, their type of wavenumber–frequency analysis only examined signals that propagate eastward at typical Kelvin wave phase speeds. Therefore, this analysis excludes any westward-moving features that might be forced by the CCKW. In contrast, the composites in Fig. 6 are able to capture the evolution of both eastward- and westward-propagating structures within the water vapor anomaly field. Figure 6 shows unfiltered TCWV anomalies (shaded) averaged over each CCKW lag. Significant negative

TCWV anomalies are observed within the convectively suppressed phase of the CCKW and significant positive TCWV anomalies are collocated within the convectively active phase of the CCKW throughout all lags. In addition to this anomalous TCWV pattern, significant TCWV anomalies are found to occur outside of the Kelvin-filtered OLR anomalies and are observed to progress westward with time.

An area of significant negative TCWV anomalies is observed over West Africa on day -6 (Fig. 6a). Later on day -1 , this area of significant negative TCWV anomalies is located farther west over 10° – 25° N, 40° – 50° W (Figs. 6b–f). This westward-moving dry signature is hypothesized to be associated with a Saharan air layer (SAL) outbreak in some cases, and provides evidence that CCKWs may influence such events. An alternative hypothesis could be that CCKWs commonly phase with or modulate westward-propagating waves (e.g., AEWs). These westward-propagating waves could then act to initiate the SAL outbreak. A strong SAL preceded the strong CCKW that influenced the genesis of Debby (Zawislak and Zipser 2010; Zipser et al. 2009). The negative TCWV anomalies associated with the westward-moving envelope of dry air seem to interfere with the positive TCWV anomalies associated with the convectively active phase of the CCKW on day -2 (Fig. 6e). This interference results in negative TCWV anomalies occurring within the poleward half of the convectively active phase of the CCKW. One day later (day -1), significant positive TCWV anomalies progress eastward over the eastern MDR collocated with the convectively active phase of the CCKW, while negative TCWV anomalies associated with the possible SAL outbreak continue to move westward (Fig. 6f).

By day 0, no significant TCWV anomalies are observed within the eastern side of the convectively active phase of the CCKW (Fig. 6g). The lack of significant TCWV anomalies within the eastern side of the convectively active phase of the CCKW appears to occur from the superposition between the positive TCWV anomalies that are associated with the eastward-propagating CCKW and negative TCWV anomalies that are associated with a westward-propagating disturbance. By day $+1$, positive TCWV anomalies return to the eastern side of the convectively active phase of the CCKW, while no significant anomalies are observed within the western side. The western side of the convectively active phase of the CCKW is still superposed with the anomalously dry signature associated with the westward-propagating disturbance and therefore the anomalies are reduced to zero.

After the passage of the convectively active phase of the CCKW over the tropical Atlantic, areas of

significant anomalous moisture are seen to progress back toward the west (Figs. 6g–l). Therefore, TCWV increases over the tropical Atlantic during and after the passage of the convectively active phase of the CCKW. This increased moisture signature is a composed from a combination of both eastward- and westward-moving signatures.

3) LOW-LEVEL (925 HPA) RELATIVE VORTICITY

Finally, low-level (925 hPa) relative vorticity is plotted in Fig. 7 for each CCKW lag. Between days -6 and -1 , scattered areas of anomalous anticyclonic relative vorticity are observed to progress eastward with the leading suppressed phase of the CCKW (Figs. 7a–f). Over the west-northwestern MDR on day -6 , a large area of anomalous anticyclonic relative vorticity is poleward of the convectively suppressed phase of the CCKW (Fig. 7a). On day -5 , a preexisting area of anticyclonic relative vorticity over the eastern Atlantic increases in magnitude during the superposition with the convectively suppressed phase of the CCKW (Fig. 7b). This anticyclonic relative vorticity anomaly then progresses back toward the west throughout the subsequent lags (Figs. 7a–h). When compared to the composite TCWV anomalies, this westward-moving area of anomalous anticyclonic relative vorticity slightly leads the westward-moving area of anomalously dry air associated with the possible SAL outbreak discussed earlier (cf. Figs. 6a–h).

On day -3 , the convectively active phase of the CCKW is located over the MDR and a zonally oriented strip of cyclonic relative vorticity anomalies forms over the tropical Atlantic (5° – 10° N, 30° – 55° W; Fig. 7d). One day later (day -2), these positive relative vorticity anomalies amplify within the convectively active phase of the CCKW (Fig. 7e). On day -1 , the cyclonic relative vorticity anomalies reduce in magnitude and remain quasi-stationary (Fig. 7f). Anticyclonic relative vorticity anomalies that were generated over West Africa on day -3 during the passage of the suppressed phase of the CCKW (see Fig. 7d) have progressed westward and interfere with the eastward progression of cyclonic relative vorticity anomalies (Figs. 7d–f). During the following lags, this couplet of anomalous cyclonic and anticyclonic relative vorticity moves westward together across the MDR (Figs. 7g–j).

On day -1 , an area of significant anomalous cyclonic relative vorticity forms in between the leading convectively suppressed phase and the convectively active phase of the CCKW (Fig. 7f). This location is consistent with where the strongest low-level zonal convergence occurs (recall Fig. 2a). Under the superposition of the convectively active phase of the CCKW on day 0, this

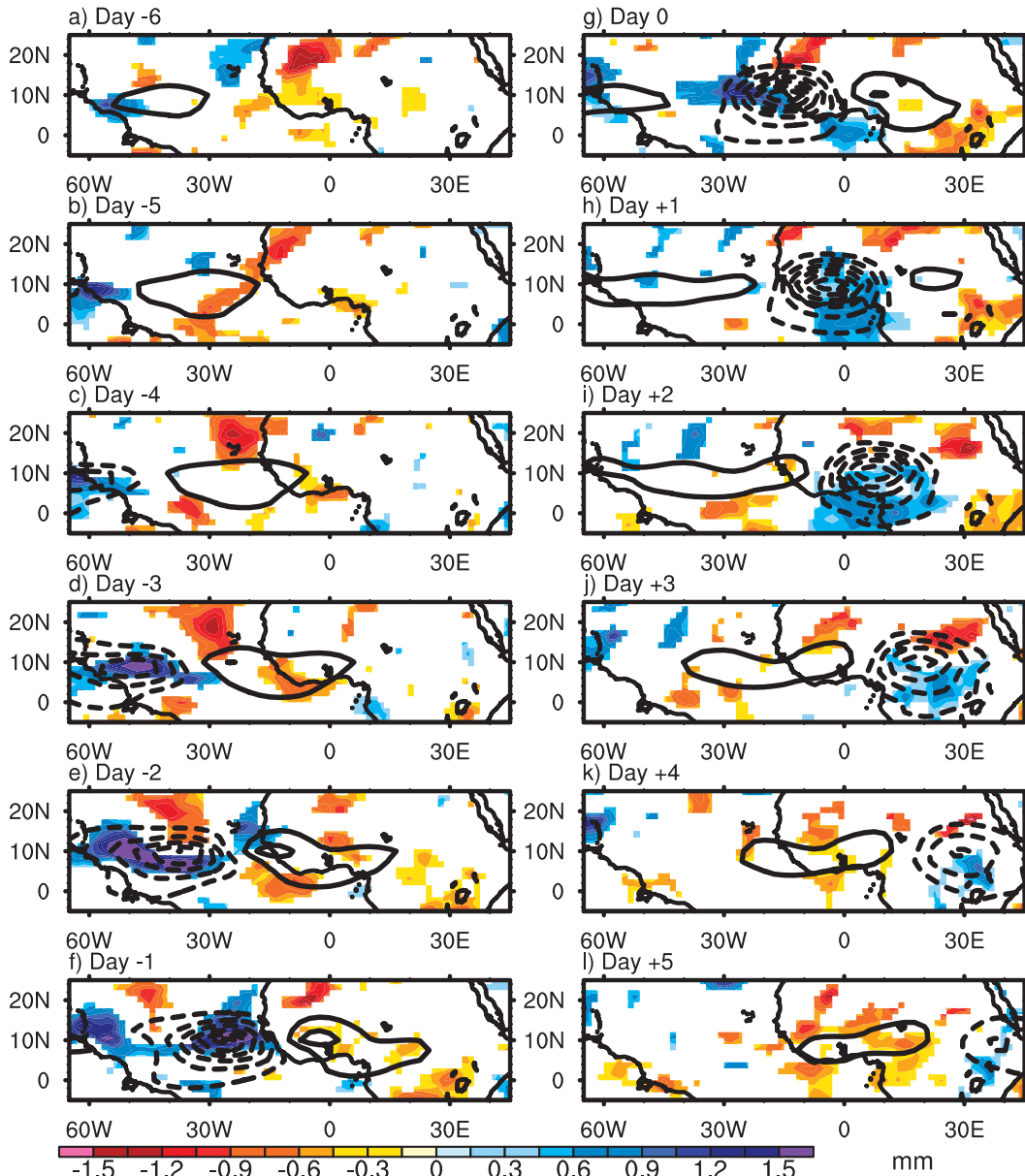


FIG. 6. Total column water vapor anomaly composite averaged over each CCKW lag. Anomalies statistically different than zero at the 95% level are shaded. Kelvin-filtered OLR anomalies are contoured if statistically different than zero at the 95% level. Negative Kelvin-filtered OLR anomalies are dashed. Shade interval is 0.15 mm; contour interval is 3 W m^{-2} .

area of anomalous cyclonic relative vorticity intensifies (Fig. 7g). This anomalous cyclonic relative vorticity did not exist on day -2 , and is suggestive that it was generated by CCKW interacting with the topography of the Guinea Highlands region. Between days $+1$ and $+5$, the convectively active phase of the CCKW propagates eastward over Africa, generating anomalous low-level cyclonic relative vorticity, which then later moves back toward the west (Figs. 7h–l).

On day $+1$, a complex pattern develops over the MDR (Fig. 7h). A wavelike pattern is expressed within the low-level relative vorticity field and consists of two separate areas of anomalous anticyclonic relative vorticity (located over 15° – 20°N , 60° – 65°W and 5° – 15°N , 40° – 50°W , respectively), with an area of anomalous cyclonic relative vorticity (10° – 15°N , 50° – 60°W) in between. Furthermore, an additional but weaker area of anomalous cyclonic relative vorticity is located over 10° – 13°N ,

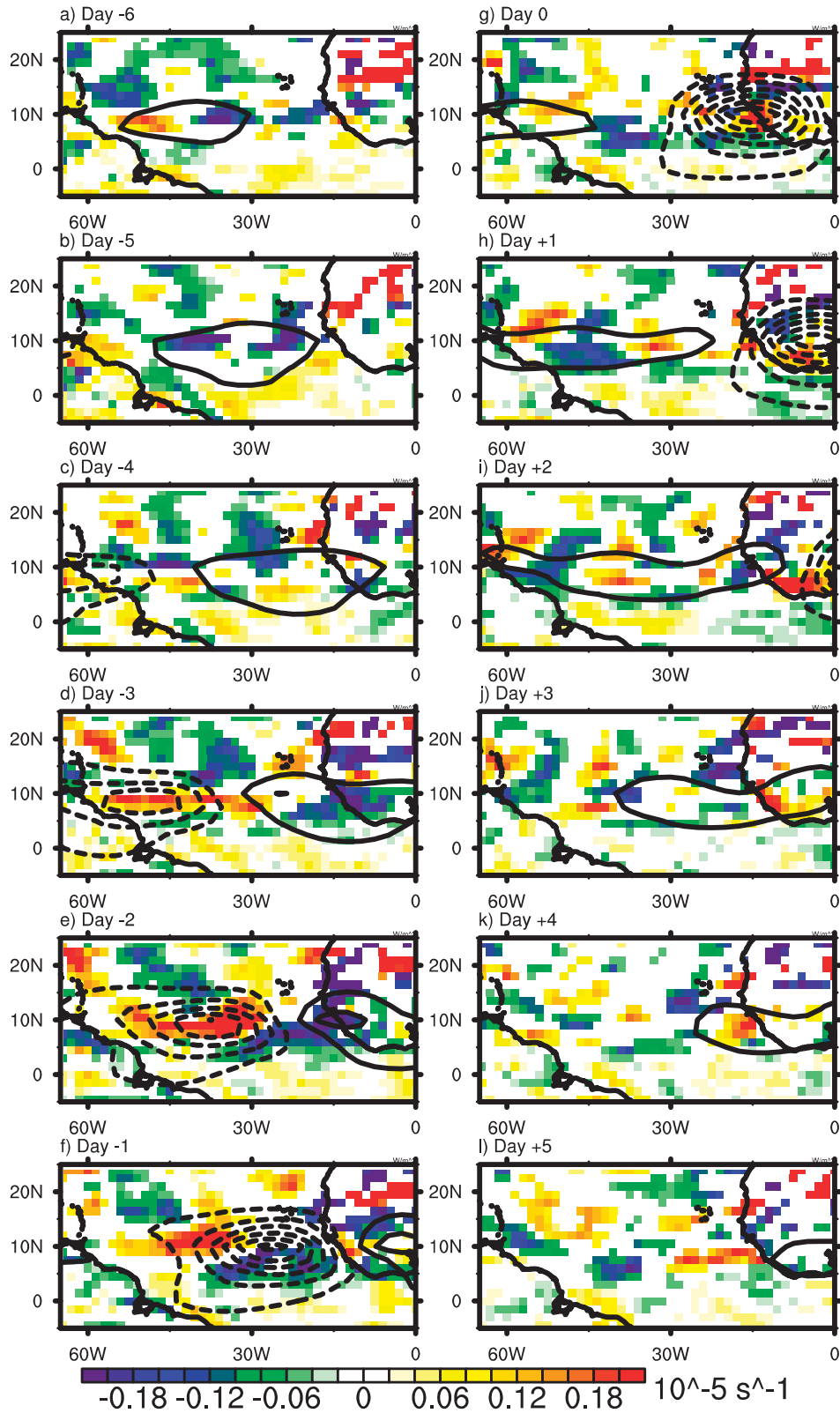


FIG. 7. 925-hPa relative vorticity anomaly composite averaged over each CCKW lag. Anomalies statistically different than zero at the 90% level are shaded. Kelvin-filtered OLR anomalies are contoured if statistically different than zero at the 95% level. Negative Kelvin-filtered OLR anomalies are dashed. Shade interval is $0.02 \times 10^{-5} \text{ s}^{-1}$; contour interval is 3 W m^{-2} .

30°–35°W. This wavelike pattern within the relative vorticity field moves westward with time and potentially represents a westward propagating train of easterly waves. To build perspective, Fig. 8 shows anomalies of Kelvin-filtered OLR (shaded) and 925-hPa streamfunction (contoured) averaged over the dates of the CCKW index. Days -2 through $+2$ are only shown to focus on the westward-propagating structures over the tropical Atlantic. Negative streamfunction anomalies (dashed contours) are observed to progress eastward with the convectively active phase of the CCKW with the exception of day -1 . On day -2 , a large couplet of negative and positive streamfunction anomalies is observed over the tropical Atlantic and West Africa (Fig. 8a). The minimum negative streamfunction anomaly is collocated with the minimum negative Kelvin-filtered OLR anomaly. The maximum positive streamfunction anomaly located within the convectively suppressed phase of the Kelvin wave, however, is located slightly to the northwest of the maximum positive Kelvin-filtered OLR anomaly.

By day -1 , the large couplet of negative and positive streamfunction anomalies is located slightly more westward than on day -2 (Fig. 8b). This westward shift of streamfunction anomalies highlights an interference pattern between a westward-propagating signature and the eastward-propagating Kelvin wave signature. Positive streamfunction anomalies are located within the convectively active phase of the CCKW because of the interference. By day 0, the anomalous streamfunction couplet is located farther westward, but reduces in horizontal extent (Fig. 8c). During this time, negative streamfunction anomalies are once again collocated with the convectively active phase of the CCKW. The anomalous streamfunction couplet over the tropical Atlantic is located farther west on day $+1$ (Fig. 8d). By day $+2$, a new area of anomalous negative streamfunction develops east of the couplet over 40°W, confirming the train of westward-propagating disturbances observed in Fig. 7.

A vertical cross section of meridional wind anomalies through 10°N on day $+2$ is used to investigate the vertical structure of the westward-propagating wave train over 30°–60°W (Fig. 9). Over West Africa, a large upper-level anticyclonic circulation is observed over a low-level cyclonic circulation. The low-level cyclonic circulation is centered over $\sim 5^\circ\text{E}$, whereas the upper-level anticyclonic circulation is centered slightly westward over $\sim 0^\circ$. Recall that the minimum negative Kelvin-filtered OLR anomaly is located over 10°E on day $+2$ (cf. Fig. 4i), therefore, it is suggested that these large circulations over Africa are a response to the CCKW passage. Over the tropical Atlantic, vertically stacked anomalies of meridional wind stretch from the surface to

250 hPa. The southerly meridional wind anomalies peak near 600 hPa, while the northerly meridional wind anomalies peak near 500 hPa, consistent with past observations of AEWs over the Atlantic (see Fig. 6 in Kiladis et al. 2006).

An alternative interpretation of the wave like disturbances that develop over the Atlantic after the passage of the CCKW is that of a possible breakdown of the Atlantic ITCZ into individual vortices. A similar scenario occurred during the observations of Nieto Ferreira and Schubert (1997) over the Pacific. Their Fig. 1 shows an east Pacific ITCZ breakdown that resulted in five tropical depressions. Further examination of this event revealed that this ITCZ breakdown occurred during the passage of the convectively active phase of a CCKW (not shown). More recently, Schreck and Molinari (2011) discussed a similar potential vorticity (PV) strip over the western Pacific that broke into two separate vortices and eventually spawned Typhoons Rammasun and Chataan. This breakdown occurred just after the passage of a series of CCKWs during an active MJO phase. The organization of deep cumulus convection within the ITCZ during a CCKW passage increases latent heat release and produces a low-level cyclonic PV anomaly, which then occasionally breaks down into individual vortices.

c. The initiation of Atlantic convectively coupled atmospheric Kelvin waves

CCKWs are commonly triggered by preexisting tropical convection, however, extratropical Rossby wave trains perturbing deep into the tropical waveguide have also been shown to initiate CCKWs (Straub and Kiladis 2003a). CCKWs that form in association with Rossby wave trains are most commonly found over the western Pacific. CCKWs found over the Atlantic have been commonly associated with pressure surges propagating from extratropical South America northward along the lee of the Andes (Liebmann et al. 2009). Similar to CCKWs found over the western Pacific, these pressure surges are associated with extratropical Rossby wave trains interacting with the Andes. When a strong mid-latitude trough propagates across the Andes, cold air is funneled down the lee of the Andes and deep into the tropics, similar to the cold-air outbreaks over the lee of the Rockies in the United States. This cold air intruding the tropics triggers an elongated band of deep convection ahead of the cold air. The remnants of this organized convection propagate toward the equator where it sets up favorable conditions for the initiation of a Kelvin wave.

In addition to CCKWs that are generated by pressure surges over South America, the strongest CCKWs that propagate over the tropical Atlantic are linked with the

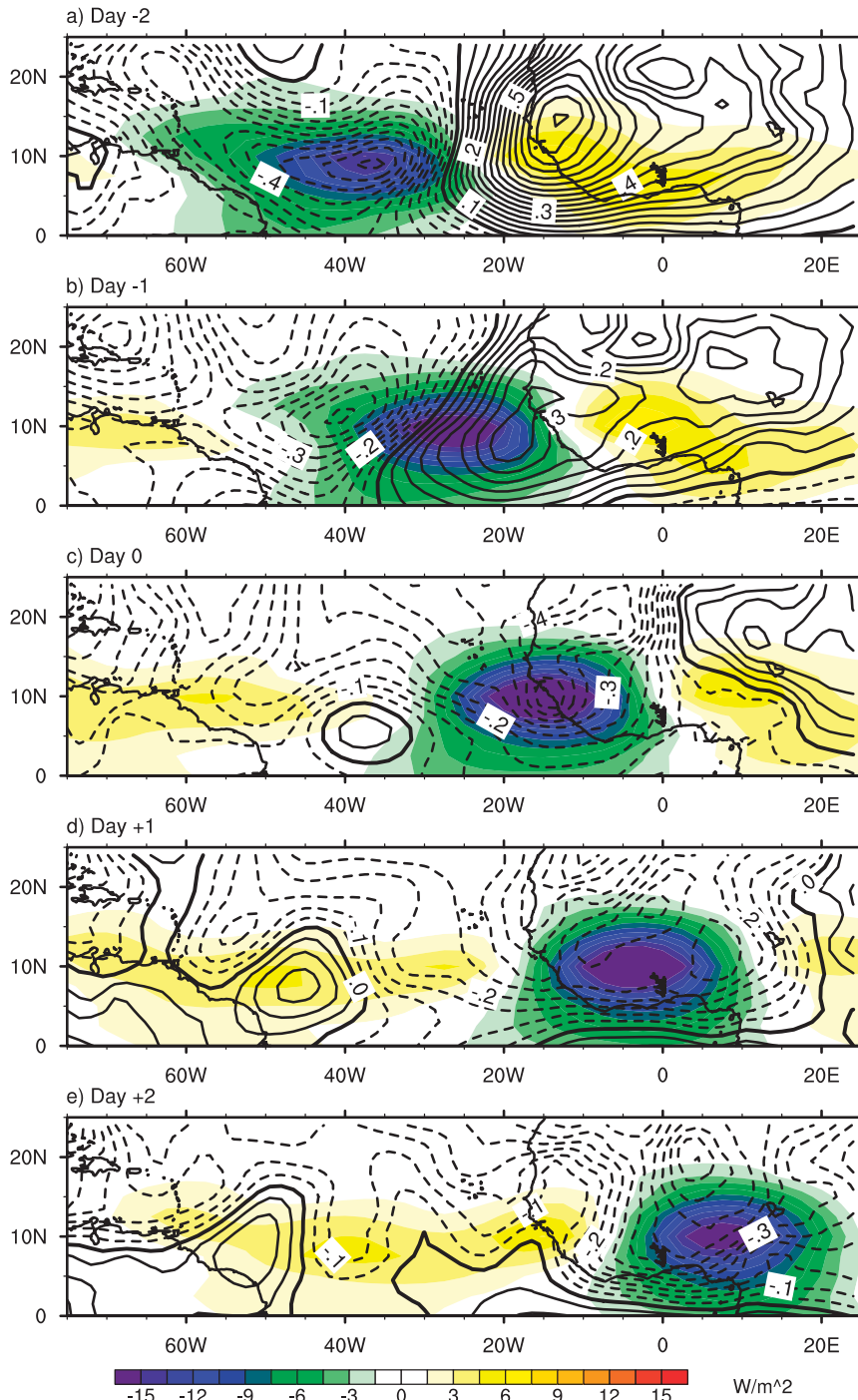


FIG. 8. 925-hPa streamfunction anomaly composite averaged over particular CCKW lags. Kelvin-filtered OLR anomalies are shaded. Stream function anomalies are contoured. Negative streamfunction anomalies are dashed. Shade interval is $1.5 W m^{-2}$; contour interval is $0.1 \times 10^6 m^2 s^{-1}$.

location of active convection associated with the MJO. Figure 10 shows a time-longitude composite of unfiltered 200-hPa velocity potential (VP) anomalies overlaid with Kelvin-filtered OLR anomalies (black contours) and

MJO-filtered OLR anomalies (orange contours) averaged over the set of dates identified using the CCKW index. In this case, negative VP anomalies represent upper-level divergence. Each variable is averaged over the 5° – $10^{\circ}N$

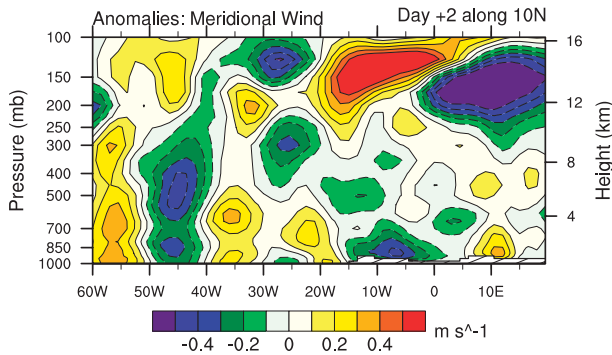


FIG. 9. A cross section of meridional wind anomalies along 10°N on day +2.

latitude band to maximize the convective signatures of CCKWs and the MJO during boreal summer. The MJO filtering is performed following the methodology of Kiladis et al. (2005), using a period of 30–96 days, with eastward wavenumbers 0–9. Recall day 0 represents the time when the minimum composite negative Kelvin-filtered OLR anomaly is located over 10°N , 15°W .

According to Fig. 10, the eastward progression of negative VP anomalies occurs in tandem with the convectively active phase of the composited CCKW (black dashed contour). An eastward progression of negative VP anomalies within the convectively active phase of the CCKW was also demonstrated by Mekonnen et al. (2008). At lag -6 over 90°W , the convectively active phase of the composited CCKW first appears over the Pacific basin. The convective signature of the CCKW occurs where the active convection associated with MJO (orange dashed contour) ceases. This result does not necessarily mean that the CCKW was generated by the active convection associated with MJO; however, it does suggest a common phasing between the two features. Furthermore, it appears that the low-frequency active convection associated with the MJO propagates eastward across the Western Hemisphere with the composited CCKW convective signature. This result suggests that the strongest CCKWs observed over the tropical Atlantic region are commonly associated with the decay of the active convective signal of the MJO over the Pacific and eastward progression over the Western Hemisphere. This result is consistent with Straub and Kiladis (2003b) and Mekonnen et al. (2008), who find that strong CCKWs over the eastern Pacific and Africa are commonly associated the demise of the MJO convective signature over the Pacific.

At lag +6, the convectively active phase of the composited CCKW is located over the Indian Ocean. After the passage of the composited CCKW, a new MJO convective signal forms and later propagates eastward

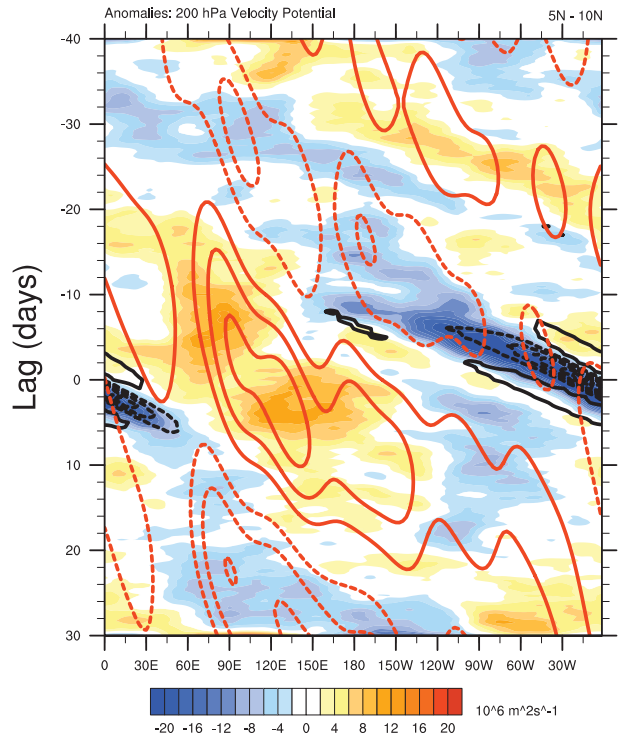


FIG. 10. A time-longitude composite of unfiltered 200-hPa velocity potential anomalies. A 5-day running average was applied to temporally smooth the velocity potential data. Day 0 is when the minimum negative Kelvin-filtered OLR anomaly is located over 10°N , 15°W . Kelvin-filtered OLR is represented by the black contours and are drawn every 3 W m^{-1} . MJO-filtered OLR is represented by the orange contours and are drawn every 0.5 W m^{-2} . Negative filtered OLR anomalies are dashed. All variables were averaged over the $5^{\circ}\text{--}10^{\circ}\text{N}$ latitude band.

throughout the later lags. This result suggests that CCKWs might be an important feature in the genesis of the MJO. This result is consistent with the findings of Straub et al. (2006). Furthermore, this result implies CCKWs that are associated with the decay of the convectively active phase of the MJO over the Pacific might occasionally be involved with the generation of a new MJO convective signature over the Indian Ocean roughly two weeks later.

4. Discussion

Ventrice et al. (2012) showed that over the entire tropical Atlantic, just prior to the passage of the convectively active phase of the CCKW, there is reduced tropical cyclogenesis frequency. After the passage, there is more frequent genesis. We have highlighted here how the passage of CCKWs impact vertical wind shear, moisture, and low-level relative vorticity. These factors are now summarized in turn to explain the tropical

cyclogenesis frequency variations noted by Ventrice et al. (2012).

a. Vertical wind shear

Over the western tropical Atlantic, genesis is infrequent prior to the passage of the minimum Kelvin-filtered OLR anomaly when the climatological westerly shear is increased by the Kelvin wave-induced westerly shear. But after the passage of the minimum Kelvin-filtered OLR anomaly over the western tropical Atlantic, Kelvin wave-induced easterly shear reduces the climatological westerly shear consistent with the observation of more frequent genesis events there. Over the eastern Atlantic, genesis is less frequent just prior to the passage of the minimum Kelvin-filtered OLR anomaly as Kelvin wave induced westerly shear reduces the climatological easterly shear. After the passage of the minimum Kelvin-filtered OLR anomaly, more frequent genesis events are observed as Kelvin wave-induced easterly shear over the eastern MDR increases the climatological easterly shear. In a comparison study between nondeveloping and developing AEWs, Hopsch et al. (2010) found that AEWs that develop over the tropical Atlantic occur when there is increased 850–200-hPa vertical wind shear over the southern MDR. Our results are consistent with Hopsch et al. (2010), such that 925–200-hPa vertical wind shear increases over the southern MDR after the passage of the CCKW during a time of frequent Atlantic tropical cyclogenesis.

The fact that, in contrast to the western tropical Atlantic, tropical cyclogenesis over the eastern tropical Atlantic is found to be favored when the CCKW enhances the local shear deserves comment. Tuleya and Kurihara (1981) performed a modeling study showing that mean easterly shear is more favorable for tropical cyclogenesis than westerly shear with respect to a westward-moving wave in the Northern Hemisphere. They find that the easterly shear value most favorable for the early development of the tropical cyclone was 15 m s^{-1} . This result is consistent with Figs. 3 and 4, highlighting an 11–18 m s^{-1} mean easterly shear value over the eastern Atlantic after the passage of the minimum Kelvin-filtered OLR anomaly. Nolan and McGauley (2012) find discrepancies between their idealized simulations and statistical favorability of easterly wind shear for genesis and suggest that the strong correlation between easterly shear and other favorable factors, such as increased thermodynamic favorability, or with geographical areas that have stronger initiating disturbances could be responsible for the relationship.

It is possible that the anomalous easterly shear phase of the CCKW seen here, west of the anomalous CCKW convection, is associated with a region of enhanced

AEW activity (cf. Mekonnen et al. 2008; Leroux et al. 2010). This increased AEW activity may be more important for tropical cyclogenesis frequency there than the shear. This aspect of CCKWs will be explored in a future paper.

b. Moisture

Two to three days before the passage of the convectively active phase of a CCKW, anomalously dry air is advected westward from West Africa over the MDR. One possible source of the dry air is from the Sahara, but midlatitude influences may also be playing a role (Braun 2010). It is hypothesized that the low-level dynamical structure of the CCKW influences SAL outbreaks due to enhancement of lower-tropospheric easterly flow within the convectively suppressed phase of the CCKW. The anomalously dry air also likely contributes in suppressing deep convection over the MDR prior to the passage of the convectively active phase of the CCKW, which would tend to reduce the frequency of genesis.

Moisture significantly increases over the tropical Atlantic during the passage of the convectively active phase of the CCKW. This moist signature progresses eastward with the convectively active phase of the CCKW. After the passage of the convectively active phase of the CCKW over the tropical Atlantic, areas of significant moist anomalies progress back toward the west. Through the combination of eastward and westward moisture signatures over the tropical Atlantic, moisture is increased over the tropical Atlantic over an 8–9-day period.

Agudelo et al. (2010) suggested that the likelihood of a developing AEW increases when the wave enters an environment characterized by preexisting moist convection. Consistent with that, Hopsch et al. (2010) conclude that the presence of dry mid- to upper-level air just ahead of the nondeveloping AEW composite was a major limitation for that wave to undergo tropical cyclogenesis. Mid- to upper-level dry air is less likely to be located over the tropical Atlantic during the passage of the convectively active phase of a CCKW. Therefore, any AEWs propagating off the coast of West Africa during a time when the convectively active phase of a CCKW is located over the tropical Atlantic will soon enter an environment where moist convection is present. Following the arguments presented by Hopsch et al. (2010) and Agudelo et al. (2010), these AEWs will be more likely to develop thereafter.

c. Low-level relative vorticity

Anomalous anticyclonic relative vorticity is generated within the leading suppressed phase of the CCKW and is assumed to contribute to the anomalously low genesis activity then. Furthermore, a broad area of anomalous

anticyclonic relative vorticity is observed to progress westward across the tropical Atlantic prior to the passage of the convectively active phase of the CCKW over the eastern tropical Atlantic. This area of anomalous anticyclonic relative vorticity slightly leads the anomalous dry SAL air that progresses westward discussed above.

During the passage of the convectively active phase of the CCKW, a zonally oriented strip of low-level cyclonic relative vorticity develops over the tropical Atlantic. This strip of cyclonic relative vorticity later becomes part of a wavelike pattern that develops over the tropical Atlantic after the passage of the convectively active phase of the CCKW. This wavelike pattern progresses westward throughout subsequent lags and is associated with a train of westward-propagating easterly waves. Kiladis et al. (2009) discusses the amplification of WIG waves during the passage of a CCKW, but these westward-propagating disturbances have a wavelength of ~ 2500 km and a westward phase speed of $\sim 7\text{--}8$ m s $^{-1}$, implying that they are more similar to easterly waves (cf. Fig. 14 in Mekonnen et al. 2008). The increased low-level cyclonic flow and increased easterly wave activity over the tropical Atlantic during and after the passage of the CCKW occurs during a time when genesis is most frequent.

d. Summary

The overall low tropical cyclogenesis activity observed by Ventrice et al. (2012) ahead of the convectively active phase of the CCKW arises from unfavorable large-scale environmental conditions (including enhanced westerly vertical wind shear and reduced easterly vertical wind shear, reduced atmospheric moisture, and anomalous anticyclonic low-level relative vorticity), along with the influence of the westward-moving SAL or midlatitude dry air outbreak (see Dunion and Velden 2004). The increasing trend of tropical cyclogenesis events observed in Fig. 9 of Ventrice et al. (2012) between days 0 and +2 occurs from the combination of the direct enhancement of convection associated with the convectively active phase of a CCKW, as well as more favorable large-scale environmental conditions (reduced westerly vertical wind shear and enhanced easterly vertical wind shear, increased atmospheric moisture, and anomalous cyclonic low-level relative vorticity) for tropical cyclogenesis.

5. Conclusions

Strong CCKWs are commonly observed over the tropical Atlantic during Northern Hemisphere boreal summer. CCKWs have distinct vertical structures that are expressed in zonal wind, temperature, and specific

humidity. It has been demonstrated that CCKWs impact the large-scale environmental conditions associated with tropical cyclogenesis.

This analysis provides information pertaining to the role of CCKWs on weather variability over the tropical Atlantic. From an operational forecasting perspective, in addition to extreme precipitation events over tropical regions such as Africa (e.g., Mekonnen et al. 2008), we recommend that CCKWs be monitored daily for their potential influence on tropical cyclogenesis over the MDR (Ventrice et al. 2012). Our results suggest a common phasing with the active convection associated with the MJO. By assessing the particular phase of the real-time multivariate MJO (RMM) phase space (e.g., Wheeler and Hendon 2004), and the location of active convection associated with a CCKW, the possibility exists to make useful long-range predictions of anomalously active or suppressed Atlantic tropical cyclogenesis activity.

A limited number of methods have been attempted to observe and forecast CCKWs in real time. Wheeler and Weickmann (2001) investigated forecasting convectively coupled tropical wave modes by using their real-time filtering approach. This filtering approach is achieved by filtering OLR anomaly data with zero padding applied to all future times, and then made predictions through simple extrapolation. This methodology successfully captures lower-frequency phenomena, such as equatorial Rossby waves and the MJO. Depending on the resolution of the dataset being used, this method tends to dampen higher-frequency wave modes such as CCKWs too fast and sometimes limits the usefulness of the forecast. Roundy et al. (2009) provide a statistical approach to real-time filter convectively coupled tropical waves by using an algorithm that combines filtering in the wavenumber–frequency domain with time-extended empirical orthogonal functions. This methodology avoids the distortion at the end of the dataset observed in data filtered in the wavenumber–frequency domain without the addition of zero-padding future times and acts to statistically predict future CCKWs reasonably well. We recommend the use of these real-time space–time filtering approaches as compliments to numerical weather prediction forecasts given the well-known problems that dynamical models have with the representation of convectively coupled waves in the tropics (Lin et al. 2006).

Acknowledgments. We extend our gratitude to NASA for Grant NNX09AD08G, which supported this research. We would like to credit the European Centre for Medium-Range Weather Forecasts for the use of the ECMWF-Interim dataset. We also express gratitude to Paul Roundy for personal communications. Furthermore,

we thank Matthew Janiga for assistance in data analysis and Kyle Griffin and two anonymous reviewers who have made insightful contributions toward a previous version of the manuscript. Interpolated OLR data were provided by the NOAA/OAR/ESRL PSD, Boulder, Colorado, from their website (<http://www.esrl.noaa.gov/psd/>).

REFERENCES

- Agudelo, P. A., C. D. Hoyos, J. A. Curry, and P. J. Webster, 2010: Probabilistic discrimination between large-scale environments of intensifying and decaying African easterly waves. *Climate Dyn.*, **36**, 1379–1401.
- Aiyyer, A., and C. D. Thorncroft, 2011: Interannual-to-multidecadal variability of vertical shear and tropical cyclone activity. *J. Climate*, **24**, 2949–2962.
- Andrews, D. G., J. R. Holton, and C. B. Leovy, 1987: *Middle Atmosphere Dynamics*. Academic, 489 pp.
- Braun, S. A., 2010: Reevaluating the role of the Saharan air layer in Atlantic tropical cyclogenesis and evolution. *Mon. Wea. Rev.*, **138**, 2007–2037.
- Dias, J., and O. Pauluis, 2009: Convectively coupled waves propagating along an equatorial ITCZ. *J. Atmos. Sci.*, **66**, 2237–2255.
- Dunion, J. P., and C. S. Velden, 2004: The impact of the Saharan air layer on Atlantic tropical cyclone activity. *Bull. Amer. Meteor. Soc.*, **85**, 353–365.
- Ferguson, J., B. Khouider, and M. Namazi, 2009: Two-way interactions between equatorially-trapped waves and the barotropic flow. *Chin. Ann. Math.*, **30**, 539–568.
- Gill, A. E., 1980: Some simple solutions for heat-induced tropical circulation. *Quart. J. Roy. Meteor. Soc.*, **106**, 447–462.
- Goldenberg, S. B., and L. J. Shapiro, 1996: Physical mechanisms for the association of El Niño and West African rainfall with Atlantic major hurricane activity. *J. Climate*, **9**, 1169–1187.
- Gray, W. M., 1968: Global view of the origin of tropical disturbances and storms. *Mon. Wea. Rev.*, **96**, 669–700.
- , 1984: Atlantic seasonal hurricane frequency. Part I: El Niño and 30 mb Quasi-Biennial Oscillation influences. *Mon. Wea. Rev.*, **112**, 1649–1668.
- , 1988: Environmental influences on tropical cyclones. *Aust. Meteor. Mag.*, **36**, 127–139.
- , 1998: The formation of tropical cyclones. *Meteor. Atmos. Phys.*, **67**, 37–69.
- Gruber, A., 1974: The wavenumber-frequency spectra of satellite-measured brightness in the tropics. *J. Atmos. Sci.*, **31**, 1675–1680.
- Hopsch, S. B., C. D. Thorncroft, and K. R. Tyle, 2010: Analysis of African easterly wave structures and their role influencing tropical cyclogenesis. *Mon. Wea. Rev.*, **138**, 1399–1419.
- Kikuchi, K., and B. Wang, 2010: Spatiotemporal wavelet transform and the multiscale behavior of the Madden–Julian oscillation. *J. Climate*, **23**, 3814–3834.
- Kiladis, G. N., K. H. Straub, and P. T. Haertel, 2005: Zonal and vertical structure of the Madden–Julian Oscillation. *J. Atmos. Sci.*, **62**, 2790–2809.
- , C. D. Thorncroft, and N. M. J. Hall, 2006: Three dimensional structure and dynamics of African easterly waves. Part I: Observations. *J. Atmos. Sci.*, **63**, 2212–2230.
- , M. C. Wheeler, P. T. Haertel, K. H. Straub, and P. E. Roundy, 2009: Convectively coupled equatorial waves. *Rev. Geophys.*, **47**, RG2003, doi:10.1029/2008RG000266.
- Klotzbach, P. J., 2010: On the Madden–Julian Oscillation–Atlantic hurricane relationship. *J. Climate*, **23**, 282–293.
- , and W. M. Gray, 2008: Multidecadal variability in North Atlantic tropical cyclone activity. *J. Climate*, **21**, 3929–3935.
- Laing, A. G., R. E. Carbone, V. Levizzani, and J. D. Tuttle, 2011: Cycles and propagation of deep convection over equatorial Africa. *Mon. Wea. Rev.*, **139**, 2832–2853.
- Leroux, S., N. Hall, and G. Kiladis, 2010: A climatological study of transient-mean flow interactions over West Africa. *Quart. J. Roy. Meteor. Soc.*, **136**, 397–410.
- Liebmann, B., and C. A. Smith, 1996: Description of a complete (interpolated) outgoing long-wave radiation dataset. *Bull. Amer. Meteor. Soc.*, **77**, 1275–1277.
- , G. N. Kiladis, L. M. V. Carvalho, C. Jones, C. S. Vera, I. Bladé, and D. Allured, 2009: Origin of convectively coupled Kelvin waves over South America. *J. Climate*, **22**, 300–315.
- Lin, J.-L., and Coauthors, 2006: Tropical intraseasonal variability in 14 IPCC AR4 climate models. Part I: Convective signals. *J. Climate*, **19**, 2665–2690.
- Lindzen, R. S., 1967: Planetary waves on beta-planes. *Mon. Wea. Rev.*, **95**, 441–451.
- , and T. Matsuno, 1968: On the nature of large scale wave disturbances in the equatorial lower stratosphere. *J. Meteor. Soc. Japan*, **46**, 215–221.
- Maloney, E. D., and J. Shaman, 2008: Intraseasonal variability of the West African Monsoon and Atlantic ITCZ. *J. Climate*, **21**, 2898–2918.
- Matsuno, T., 1966: Quasi-geostrophic motions in the equatorial area. *J. Meteor. Soc. Japan*, **44**, 25–43.
- Mekonnen, A., C. D. Thorncroft, A. R. Aiyyer, and G. N. Kiladis, 2008: Convectively coupled Kelvin waves over tropical Africa during the boreal summer: Structure and variability. *J. Climate*, **21**, 6649–6667.
- Mounier, F., G. N. Kiladis, and S. Janicot, 2007: Analysis of the dominant mode of convectively coupled Kelvin waves in the West African monsoon. *J. Climate*, **20**, 1487–1503.
- Nieto Ferreira, R., and W. H. Schubert, 1997: Barotropic aspects of ITCZ breakdown. *J. Atmos. Sci.*, **54**, 261–285.
- Nolan, D. S., and M. G. McGauley, 2012: Tropical cyclogenesis in wind shear: Climatological relationships and physical process. *Cyclones: Formation, Triggers, and Control*, K. Oouchi and H. Fudeyasu, Eds., Nova Science Publishers.
- Nguyen, H., and J.-P. Duvel, 2008: Synoptic wave perturbations and convective systems over equatorial Africa. *J. Climate*, **21**, 6372–6388.
- Roundy, P. E., 2008: Analysis of convectively coupled Kelvin waves in the Indian Ocean MJO. *J. Atmos. Sci.*, **65**, 1342–1359.
- , and W. M. Frank, 2004: A climatology of waves in the equatorial region. *J. Atmos. Sci.*, **61**, 2105–2132.
- , C. J. Schreck III, and M. A. Janiga, 2009: Contributions of convectively coupled equatorial Rossby waves and Kelvin waves to the real-time multivariate MJO indices. *Mon. Wea. Rev.*, **137**, 469–478.
- Schreck, III, C. J., and J. Molinari, 2011: Tropical cyclogenesis associated with Kelvin waves and the Madden–Julian oscillation. *Mon. Wea. Rev.*, **139**, 2723–2734.
- Simmons, A., S. Uppala, D. Dee, and S. Kobayashi, 2007: ERA Interim: New ECMWF reanalysis products from 1989 onwards. *ECMWF Newsletter*, No. 110, ECMWF, Reading, United Kingdom, 25–35.
- Straub, K. H., and G. N. Kiladis, 2002: Observations of a convectively coupled Kelvin waves in the eastern Pacific ITCZ. *J. Atmos. Sci.*, **59**, 30–53.

- , and —, 2003a: Extratropical forcing of convectively coupled Kelvin waves during austral winter. *J. Atmos. Sci.*, **60**, 526–543.
- , and —, 2003b: Interactions between the boreal summer intraseasonal oscillation and higher frequency tropical wave activity. *Mon. Wea. Rev.*, **131**, 945–960.
- , and —, 2003c: The observed structure of convectively coupled Kelvin waves: Comparison with simple models of coupled wave instability. *J. Atmos. Sci.*, **60**, 1655–1668.
- , —, and P. E. Ciesielski, 2006: The role of equatorial waves in the onset of the South China Sea summer monsoon and the demise of El Niño during 1998. *Dyn. Atmos. Oceans*, **42**, 216–238.
- Takayabu, Y. N., 1994: Large-scale cloud disturbances associated with equatorial waves. Part I: Spectral features of the cloud disturbances. *J. Meteor. Soc. Japan*, **72**, 433–448.
- , and M. Murakami, 1991: The structure of super cloud clusters observed in 1–20 June 1986 and their relationship to easterly waves. *J. Meteor. Soc. Japan*, **69**, 105–125.
- Tuleya, R. E., and Y. Kurihara, 1981: A numerical study of the effects of environmental flow on tropical storm genesis. *Mon. Wea. Rev.*, **109**, 2487–2506.
- Tulich, S. N., and G. N. Kiladis, 2012: Squall lines and convectively coupled gravity waves in the tropics: Why do most cloud systems move westward? *J. Atmos. Sci.*, in press.
- Ventrice, M. J., C. D. Thorncroft, and P. E. Roundy, 2011: The Madden–Julian oscillation’s influence on African easterly waves and downstream tropical cyclogenesis. *Mon. Wea. Rev.*, **139**, 2704–2722.
- , —, and M. A. Janiga, 2012: Atlantic tropical cyclogenesis: A three-way interaction between an African easterly wave, diurnally varying convection, and a convectively coupled atmospheric Kelvin wave. *Mon. Wea. Rev.*, **140**, 1108–1124.
- Vizy, E. K., and K. H. Cook, 2009: Tropical storm development from African easterly waves in the eastern Atlantic: A comparison of two successive waves using a regional model as part of NASA AMMA 2006. *J. Atmos. Sci.*, **66**, 3313–3334.
- Wang, H., and R. Fu, 2007: The influence of Amazon rainfall on the Atlantic ITCZ through convectively coupled Kelvin waves. *J. Climate*, **20**, 1188–1201.
- Wheeler, M., and G. N. Kiladis, 1999: Convectively coupled equatorial waves: Analysis of clouds and temperature in the wavenumber–frequency domain. *J. Atmos. Sci.*, **56**, 374–399.
- , and K. M. Weickmann, 2001: Real-time monitoring and prediction of modes of coherent synoptic to intraseasonal tropical variability. *Mon. Wea. Rev.*, **129**, 2677–2694.
- , and H. H. Hendon, 2004: An all-season real-time multivariate MJO index: Development of an index for monitoring and prediction. *Mon. Wea. Rev.*, **132**, 1917–1932.
- , G. N. Kiladis, and P. J. Webster, 2000: Large-scale dynamical fields associated with convectively coupled equatorial waves. *J. Atmos. Sci.*, **57**, 613–640.
- Zangvil, A., 1975: Temporal and spatial behavior of large-scale disturbances in tropical cloudiness deduced from satellite brightness data. *Mon. Wea. Rev.*, **103**, 904–920.
- Zawislak, J., and E. J. Zipser, 2010: Observations of seven African easterly waves in the east Atlantic during 2006. *J. Atmos. Sci.*, **67**, 26–43.
- Zipser, E. J., and Coauthors, 2009: The Saharan air layer and the fate of African easterly waves—NASA’s AMMA field study of tropical cyclogenesis. *Bull. Amer. Meteor. Soc.*, **90**, 1137–1156.